Machine learning exploration of the direct and indirect roles of Fe impregnation on Cr(VI) removal by engineered biochar

Xinzhe Zhu [a], Zibo Xu [a], Siming You [b], Michael Komárek [c], Daniel S. Alessi [d], Xiangzhou Yuan [e,f], Kumuduni Niroshika Palansooriya [e], Yong Sik Ok [e], Daniel C.W. Tsang [a,*]

[a] Department of Civil and Environmental Engineering, The Hong Kong Polytechnic University, Hung Hom, Kowloon, Hong Kong, China

[b] University of Glasgow, James Watt School of Engineering, Glasgow, G12 8QQ, UK

[c] Faculty of Environmental Sciences, Czech University of Life Sciences, Kamýcká 129, 165 00 Prague-Suchdol, Czech Republic

[d] Department of Earth and Atmospheric Sciences, University of Alberta, Edmonton, Canada

[e] Korea Biochar Research Center, APRU Sustainable Waste Management Program & Division of Environmental Science and Ecological Engineering, Korea University, Seoul 02841, Republic of Korea

[f] R&D Centre, Sun Brand Industrial Inc., Jeollanam-do, 57248, Republic of Korea

*Corresponding author: dan.tsang@polyu.edu.hk

Abstract

Data mining and knowledge discovery by machine learning (ML) have recently come into application in environmental remediation, especially the exploration for the multifactorial process such as hexavalent chromium [Cr(VI)] removal by iron-biochar composite (Fe-BC). The Cr(VI) removal capacity of Fe-BC was concurrently controlled by impregnated iron species (Fe^0/Fe^{2+}/Fe^{3+}), carbon properties, and iron-carbon interactions, while the current lab-scale research could hardly untangle the overall relationships with the Cr(VI) removal experiments of one or several Fe-BCs under different research frameworks. Herein, we investigated the impacts of various microscopic material properties of Fe-BC on aqueous Cr(VI) removal by ML approach and highlighted the variations of biochar properties after iron impregnation. Our results suggested that the direct impacts of impregnated-iron contents on the Cr(VI) removal were limited, possibly related to undistinguished Fe species in the ML models, in which the roles of different iron species on Cr(VI) removal might be counteracted. Instead, the impacts of impregnated iron on the Cr(VI) removal were embodied indirectly by altering the biochar properties. Surface oxygen-containing functional groups (SOFGs) contents on biochar played a pivotal role in Cr(VI) removal according to the ML models. The condensed polyaromatic carbon matrices of BC and Fe-BC with a high content of non-polar carbon were also proved to be conducive to Cr(VI) removal. The ML models developed in this study consider surface functionalities information of BC and Fe-BC and offer a more accurate prediction for Cr(VI) removal, and the information mining behind models can act as a vital reference for the rational design of engineered biochar to remove aqueous Cr(VI).

Keywords: Iron-biochar composite; Hexavalent chromium; Redox properties; Sustainable waste management; Environmental remediation; Machine learning.

1. Introduction

Chromium (Cr) is a toxic pollutant that mainly derives from industrial activities such as mining, leather tannery, and metallurgy [1, 2]. Cr primarily exists as two species in the environment, soluble hexavalent chromium [Cr(VI)] (*i.e.,* $HCrO_4^-$, $Cr_2O_7^{2-}$ and CrO_4^{2-}) with higher toxicity and trivalent chromium [Cr(III)] with less hazard and mobility [3]. Therefore, turning Cr(VI) into Cr(III) by a reduction process followed by Cr(III) sorption/precipitation is a promising strategy to immobilize Cr(VI) pollutants in the environment [4-6]. Among various methods, biochar (BC) and iron-biochar (Fe-BC) have been demonstrated to be promising materials for the remediation of Cr(VI)-containing wastewater due to many advantages, including high redox potential, abundant sorption sites, ready availability of renewable feedstock, and easy separation/recycling [7, 8]. The ever-increasing number of articles has also proved the significant prospects of removing Cr(VI) by BC and Fe-BC (**Fig. S1**).

Fe-BC can be synthesized by using BC as a porous carbon skeleton to disperse and stabilize iron particles [8]. The removal of Cr(VI) with Fe-BC was concurrently influenced by biochar (*e.g.,* surface functional groups and porous structure characteristics) and impregnated iron minerals (*e.g.,* contents and species of iron minerals) [7, 9]. Interactions between biochar and iron minerals would further influence the properties of both carbon and iron phases in the Fe-BC. For instance, impregnated iron can alter the surface chemistry and porous structure of biochar support [7], which is critical for the Cr(VI) removal process. The dissolution-precipitation processes of iron will also be affected by the biochar matrices [10, 11], and the dissolved iron often manifests higher reactivity for Cr(VI) removal [12]. If the reciprocal

actions between iron species and carbon structure are ignored, some contrasting conclusions about the roles of iron on Cr(VI) removal by Fe-BC would be drawn in different experiments. For example, the inhibition of Cr(VI) reduction by Fe-BC was reported due to surface coverage and oxidizing capacity of iron [12], while the shuttling effect and reduction reactivity of iron were observed to enhance Cr(VI) removal by Fe-BC [13]. Therefore, there is an urgent need for an overall investigation into the influences of various factors on Cr(VI) removal capacity by Fe-BC under identical assessment frameworks, and the associated influences of impregnated iron on biochar properties should be properly recognized. The common control-variable experimental methods are time-consuming and costly, limiting the holistic exploration of a wide range of factors. Moreover, individual lab-scale research could hardly untangle the overall relationships in the Cr(VI) removal with one or several Fe-BC under different experimental frameworks.

With the accumulation of experimental data on Cr(VI) removal by BC and Fe-BC, machine learning (ML) can serve as an effective tool to explore the multivariate relationships by building accurate prediction models [14-16]. The ML models can also identify the relative importance and influential modes of these factors on the targets based on the rapid development of interpretable ML algorithms (*e.g.*, random forest (RF)) [17]. Recent studies have confirmed the competence of ML in predicting the adsorption capacity of metals and organic pollutants on carbonaceous materials based on the adsorption conditions, adsorbents properties, and nature of contaminants [18-21], and mining information from the "black-box" models [19].

Nevertheless, the available ML research primarily focused on the easily accessible macroscopic properties of BC, such as the proportion of bulk element compositions [18, 22],

while the microscopic surface characteristics (*e.g.*, surface elemental compositions and relative proportion of different surface functional groups) were overlooked. Such microscopic information of biochar surface is undeniably critical for pollutant removal, especially for the Cr(VI) removal through the adjoint redox and sorption processes [3, 23]. It has been demonstrated that the adsorption capacity of biochar for pollutants displayed significantly higher correlation coefficients with the surface polarity (*i.e.*, (N+O)/C) as indicated by X-ray photoelectron spectroscopy (XPS) than the bulk polarity determined with elemental analyzer [24]. Moreover, the relative proportion of surface oxygen-containing functional groups (SOFGs, *e.g.*, distinguishing C−O and C=O moieties) may provide more explicit information about Cr(VI) removal than the total O moiety that is collectively represented by the bulk oxygen content on biochar [25]. Another limitation of current ML models may reside in using the factors (*e.g.*, ion exchange capacity) that are not suitable to be directly manipulated as model inputs [18], which fail to offer a detailed guidance for biochar preparation.

In view of the limitations of experimental research in dealing with multifactorial relationships, the lack of microscopic biochar properties considered in current ML studies, and our hypothesis-driven demand of exploring the impacts of iron impregnation on biochar properties, we developed new ML models with RF algorithm and literature summary in this study to: (i) predict the Cr(VI) removal capacity of pristine BC and Fe-BC based on microscopic biochar properties and reaction conditions; (ii) evaluate the direct role of the iron content in the removal capacity of Cr(VI); and (iii) estimate the indirect impact of iron on Cr(VI) removal through the variation of biochar properties including surface chemical functionalities and pore structure properties. The results of this study can provide new insights into Cr(VI)

removal by BC and Fe-BC, especially for elucidating the significance of microscopic biochar properties and the interactions between the iron and biochar phases.

2. Methods

2.1. Data collection

Two categories of experimental data related to BC and Fe-BC were impartially collected from the published articles (a total of 153 journal publications) over the past decade without initial bias regarding data validity, including (i) the removal capacity of pristine BC and Fe-BC for aqueous Cr(VI), and (ii) the properties comparison of Fe-BC and corresponding pristine BC after iron impregnation. The data were directly obtained from tables or extracted from figures in the publications with Plot Digitizer 2.6.8. The Fe-BC produced by the following three widely used synthesis methods (**Fig. 1**) was focused in our study [5, 10]: (i) direct pyrolysis or hydrothermal carbonization of iron-soaked biomass (namely, Pre-), in which the pyrolysis and iron impregnation could be completed in one step and the physicochemical properties of Fe-BC could be controlled by the operating conditions and feedstock selection [9]; (ii) co-precipitation of BC and ferric/ferrous salts in an alkali solution (namely, Post-), in which the performance of Fe-BC was influenced by the properties of pre-synthesized BC and the precipitation conditions of iron [26]; (iii) liquid-phase reduction of iron by borohydride on BC surface (namely, Post/R-), in which the generation of Fe^0 by reducing agents could significantly improve the reducing capacity of Fe-BC [27, 28]. The detailed references of these collected data are summarized in the Supporting Information (**SI**, **Table S1**).

To investigate the specific roles of microscopic properties on the removal of Cr(VI), ten

factors influencing the Cr(VI) removal capacity (R, mg/g) using BC and Fe-BC were considered and divided into three categories: (i) surface chemistry characteristics from XPS analysis, including the atomic percentages of carbon (C, *at.*%) and iron (Fe, *at.*%), the atomic ratio of oxygen to carbon (O/C), and the relative proportions of non-polar C (NPC, *e.g.*, C−C, C=C, and π-π* transition), C−O (*e.g.*, phenolic, alcoholic, and etheric), C=O (*e.g.*, carbonyl, quinone, carboxyl or ester) as determined by C1s XPS; (ii) textural properties, *i.e.*, surface area calculated by Brunauer-Emmett-Teller model (S_{BET}, m^2/g); and (iii) reaction conditions, including solution pH (pH_{sol}), temperature (T, °C), and initial concentration ratio of Cr(VI) to BC or Fe-BC dosage (C_0, mg/g). Meanwhile, the data on physicochemical properties of Fe-BC and the corresponding pristine BC, including O/C, C−O/C=O (*i.e.*, the ratio of C−O to C=O), NPC, and S_{BET}, were collected to compare the variations of biochar properties before and after iron impregnation.

2.2. Machine learning models with random forest algorithm

Two ML models were developed (**Fig. 1**) with particular focus on different material properties. The basic properties (BP) of BC and Fe-BC (*i.e.*, C, O/C, Fe, and S_{BET}) and reaction conditions (*i.e.*, pH_{sol}, T, C_0) were used to construct the Model BP, while the detailed surface functionalities (SF) information of BC and Fe-BC including NPC, C−O, C=O instead of C and O/C were introduced in Model SF. It should be noted that each set of data contained valid values for all the variables in the datasets for each ML model, while the ones have been excluded in the case of missing data [29]. A total of 201 sets of data and 224 sets of data were used in Model BP and Model SF, respectively. Twenty sets of Cr(VI) removal data by BC or Fe-BC were randomly selected from common sets in the two models as the test group to directly

compare their prediction performances, while the remaining data in each model were randomly divided into the training group and the validation group with a ratio of 80:20. The data in the training group was used to train the ML models by RF algorithm, which is an ensemble ML method by averaging the performances of decision trees on various sub-sample of datasets (*i.e.*, bagging theory) to improve the predictive accuracy and control over-fitting [17, 30]. The tuned hyper-parameters in RF algorithm include the number of trees, the maximum depth of each tree, the number of features required when looking for the best split, the minimum number of samples required to split an internal node, and the minimum number of samples required to be at a leaf node [19, 29]. The parameters could be adjusted using the methods of trial-and-error and grid search according to the feedback of regression coefficient (R^2) or root-mean-square error (RMSE) in the validation group [31]. Finally, the independent data in the test group were introduced into the optimal ML models to make an unbiased evaluation for model accuracy with R^2 and RMSE (**Text S1**).

2.3. Relative importance analysis of features and partial dependence plot analysis

Relative importance analysis of features and partial dependence plot (PDP) analysis were performed to extract and mine the underlying information from the two well-developed RF models. Feature importance analysis is assessed by calculating the weighted impurity decrease of all nodes and averaging over all decision trees, which can help us understand the contribution of particular input variables to the variation of the target variables [29, 32]. However, the information derived from the rank of feature importance is limited. The dependence relationships of the target variables on important input variables are more significant, which can be visualized by the PDP analysis [33]. However, it should be noted that the PDP analysis

is more accurate in the data-intensive region. An overinterpretation of PDP analysis in the region with insufficient or almost no data should be avoided according to the density of pikes on the x-axis. The ML models were built with the Scikit-learn library in Python 3.8, and the plotting was performed using Matplotlib (version 3.4.2).

3. Results and Discussion

3.1. Higher prediction accuracy by introducing surface functional groups information into ML models

The optimal hyper-parameters of Model BP and Model SF are shown in **SI** (**Table S2**) according to the R^2 and RMSE of the validation group, while the predicted removal capacity versus the experimentally determined values are plotted in **Fig. 2**. The results suggested that Model BP, which was developed based on basic surface properties of BC and Fe-BC (*i.e.*, C, O/C, Fe, and S_{BET}) and reaction conditions, could predict the removal capacity for aqueous Cr(VI) with R^2 of 0.889 and RMSE of 13.8 mg/g in the test group (**Fig. 2a**). The acceptable predictive power of Model BP could reflect the reasonable use of surface chemical information from XPS data as model inputs [34]. Moreover, the prediction accuracy could be further improved when the relative proportion of surface functional groups was introduced into Model SF (*i.e.*, NPC, C−O, C=O, Fe, $S_{BET,}$ and reaction conditions). The predicted error (*i.e.*, RMSE) in the test group of Model SF decreased by 21.7% compared to the Model BP (**Fig. 2b**). These findings emphasized the significant roles of specific surface functional groups in predicting the removal capacity of BC and Fe-BC for aqueous Cr(VI). Relative importance analysis and PDP analysis were subsequently conducted to evaluate the roles of different factors in the ML

models.

3.2. Limited direct impacts of impregnated iron content on Cr(VI) removal

The iron content of Fe-BC showed an upward tendency to the removal capacity of Cr(VI) according to the one-factor PDP analysis (**Fig. 3a**), which could be attributed to the reduction of Cr(VI) by low-valent iron (*i.e.,* Fe^{2+} and Fe^{0}) and the enhanced electron transport by iron redox cycles [7, 35]. However, the relative importance of iron content was merely ranked as the third and fourth in Models BP and SF, respectively (**Fig. 4**). One of the critical reasons was that the total iron content could not precisely reflect the roles of different iron species on Fe-BC surface (*e.g.*, Fe_3O_4, Fe_2O_3, Fe^{2+}, Fe^{3+}, and Fe^{0}) in removing aqueous Cr(VI), such that the roles of different iron species may be counteracted and thus overlooked by the ML models. For example, Fe^{2+} and Fe^{0} with high reducing capacity can reduce Cr(VI) to Cr(III), while Fe^{3+} might inhibit the Cr(VI) reduction due to the consumption of electrons from biochar [7, 10]. In addition, the excessive iron content in some cases would result in iron aggregation and surface coverage of biochar, which might hinder the Cr(VI) removal by Fe-BC [12]. It should be noted that the increased tendency of the removal capacity due to the increase of iron content (**Fig. 3a**) represented the scenario of relatively lower iron content (*i.e.*, 0-8.3 *at.*%) because the data points of iron content above 8.3 *at.*% were sparse. Future work should focus on different ranges of iron contents and more variable iron species in the biochar composite, in which two-compartment analysis (*i.e.*, carbon structure and iron minerals) can be considered in the scenario with high iron contents. Although the direct impact of iron contents on the Cr(VI) removal is relatively limited, the indirect effects of iron by altering biochar properties could be more crucial for Cr(VI) removal capacity, as discussed in the following section.

3.3. Indirect impacts of impregnated iron on Cr(VI) removal by altering biochar properties

Impregnating biochar with iron could indirectly affect Cr(VI) removal by changing the total SOFGs content, proportions of different SOFGs, carbon structure, and surface porous properties of biochar [7]. Therefore, we scrutinized the shifts of O/C, C−O/C=O, NPC, S_{BET} after iron impregnation (**Fig. 5**), the impacts of SOFGs, carbon structure, and surface area on the Cr(VI) removal were evaluated based on the ML results.

3.3.1 Critical roles of SOFGs in Cr(VI) removal

Fig. 5a suggests that the majority of Fe-BC had higher O/C ratio than pristine BC for the three synthetic methods, in terms of bulk or surface elemental composition measured by the elemental analyzer and XPS results, respectively. The increased O/C ratio of Fe-BC may be primarily attributed to the incorporation of iron (hydr)oxide on the biochar surface [36]. The impregnation of iron would also increase the relative contents of SOFGs on the biochar surface such as -OH and -COOH due to the oxidation capacity of iron with the following reactions (Eq. 1-3) [36], where the SOFGs were critical for removing Cr(VI) based on the ML results.

$$2Fe(OH)_3 + -CH_3 \rightarrow 2Fe(OH)_2 + -CH_2-OH + H_2O \quad (1)$$

$$4Fe(OH)_3 + -CH_2-OH \rightarrow 4Fe(OH)_2 + -COOH + 3H_2O \quad (2)$$

$$2Fe(OH)_2 + -CH_2-OH \rightarrow 2Fe + -COOH + 3H_2O \quad (3)$$

In Model BP, the O/C ratio of BC and Fe-BC was the most critical factor influencing the Cr(VI) removal capacity (**Fig. 4a**) because the oxygen-containing moieties such as C−O and C=O on biochar surface could concurrently contribute to the reduction and adsorption of Cr(VI) [10]. According to the corresponding PDP analysis (**Fig. 3b**), the dependence of the removal

capacity on O/C could be further divided into three stages:

(i) The removal capacity decreased slightly with the increase of O/C ratio when O/C was less than ~0.24 (Stage I). The low O/C ratio in BC and Fe-BC resulted from the formation of well-developed graphitic carbon structures as the corresponding carbon content in the biochar was larger than 80% by tracing the collected dataset. The local highest point of Cr(VI) removal capacity at Stage I was found in the case of the lowest O/C ratio, which may be attributed to the highest amount of electron-donating carbon defects on the condensed polyaromatic carbon matrices [7, 37]. The influence of the carbon structure and carbon defects on the Cr(VI) removal is discussed in Section 3.3.2.

(ii) The removal capacity significantly increased with the increased O/C ratio from ~0.24 to ~0.32 (Stage II). At this stage, a considerable amount of SOFGs was found with a high O/C ratio, suggesting that the aliphatic carbon was the vital carbon species in the biochar. The SOFGs became the main immobilizing moieties at this stage to immobilize Cr(VI) *via* direct complexation and electron donating as well as indirect electron mediating [25, 38, 39]. The "V" transition (*i.e.*, first decrease and then increase) of Cr(VI) removal potential with the increase of O/C ratio showed by our ML models may provide a critical reference for the design of engineered biochar in the Cr(VI) decontamination.

(iii) The removal capacity decreased with the increase of O/C ratio when it was higher than ~0.32 (Stage III), which may be attributed to the poorly-developed biochar structure (C < 65%) and less accessible active sites on the biochar surface [19]. It

is noted that the minor variation of the PDP curve may result from the sparse data points when O/C ratio was higher than 0.9 [40].

The relative proportion of different SOFGs also changed after iron impregnation. Most Fe-BC, especially the Fe-BC prepared by the Pre- and Post-methods, showed lower C−O/C=O than pristine BC (**Fig. 5b**). Reduction of iron with biochar oxidation occurs during the pyrolysis process (Pre- method) or the post-impregnation process (Post- method), thus producing a higher proportion of oxidative SOFGs (*i.e.*, −C=O and −COOH) [41]. By contrast, partial Fe-BC produced by Post/R- method showed a higher C−O/C=O due to the use of reductants such as $NaBH_4$, which provided the reducing condition for the reduction of −C=O to −C−O [42].

In terms of the shift of C−O/C=O after iron impregnation, the relationship between Cr(VI) removal capacity and SOFGs was further explored by distinguishing the relative proportions of C−O and C=O in Model SF. The results indicated that the relative importance of C−O was higher than that of C=O (**Fig. 4b**). In detail, the removal capacity of Cr(VI) slightly fluctuated with the increase of C−O when it was less than ~29% based on the PDP curve (**Fig. 6a**), while a significant increase was found when the proportion of C−O was increased from ~29% to ~38%, similar to that of O/C variation at Stage II (**Fig. 3b&6a**). Our results implied that the role of C−O during Cr(VI) removal could be highlighted when the density of C−O on the biochar surface was above ~29%. The presence of C−O could directly act as the electron-donating moieties for the reduction of Cr(VI) to Cr(III) [43, 44], which has been proved by the remarkable consumption of C−O groups in biochar after Cr(VI) removal [3, 25]. Moreover, C−O in Fe-BC could couple with C=O or iron species to form redox cycles, and thus indirectly facilitate the Cr(VI) reduction [7]. However, the optimal proportion of C−O (*i.e.*, from ~29%

to ~38%) for removing aqueous Cr(VI) has not been identified or specified in the literature, requiring more experimental and theoretical research to verify in the future studies.

By comparison, the relative importance of C=O was lower by ~16% than that of C−O (**Fig. 4b)**. The higher importance of C−O than C=O in biochar for Cr(VI) may be related to the higher reduction capacity of C−O [38]. The impact patterns of C−O and C=O on the Cr(VI) removal capacity were also different (**Fig. 6a&b**). The PDP curve of C=O showed a direct increase in Cr(VI) removal with the increasing content of C=O until the proportion of C=O reached ~25%, followed by a decreasing trend. The C=O groups in the form of the carbonyl or carboxylic groups can be protonated in acidic environments, which can directly coordinate with the negatively charged Cr(VI) species by electrostatic attraction or interact with oxygen in $HCrO_4^-$ and $Cr_2O_7^{2-}$ by hydrogen bonding [45, 46]. However, C=O as an electron-lacking moiety is more inclined to accept electrons [47], so that the continuous increase of C=O may weaken the redox reaction of biochar for Cr(VI) to Cr(III) and eventually decrease the removal capacity of Cr(VI) [38]. Meanwhile, the continuous increase of C=O might also correspond to the possible decrease of relative proportion of C−O, which had a more vital role in Cr(VI) removal than C=O (**Fig. 4b**). The turning point (*i.e.*, ~25%) of C−O in Cr(VI) removal is a new observation revealed by our ML models, which may need further verification for the future design of engineered biochar.

In short, the O/C and C-O of BC and Fe-BC were crucial to Cr(VI) removal based on the ML model analysis. Iron impregnation with all three synthesis methods improved the O/C, but the Post/R- method appeared to be more liable to increasing C−O/C=O than Pre- and Post- methods (**Fig. 5**). However, the commonly used reductants (*e.g.*, $NaBH_4$ and KBH_4) in the

Post/R-method are regarded as hazardous substances [48], and thus the exploration for environmentally friendly reductants is necessary in future research to improve the performance of Fe-BC for Cr(VI) removal by forming more low-valent iron (*e.g.*, Fe^0 and Fe^{2+}) and C−O with electron-donating capacity.

3.3.2 Roles of carbon structure in Cr(VI) removal

In addition to the SOFGs, the electron transferring and reductive capacity of biochar depends on the condensed polyaromatic carbon matrices that can be readily formed at high pyrolysis temperatures [4, 49]. Therefore, we explored the influences of carbon structure on the Cr(VI) removal and the variations of C/NPC after iron impregnation. All three synthesis methods decreased the carbon content (**Fig. S2**), which was plausibly expected due to the introduction of iron species on biochar and the adjoint increased O content. However, the changes in the relative proportion of NPC (*i.e.*, the sum of C−C, C=C, and π-π* transition carbon) were variable depending on the synthesis methods. The Fe-BC produced by the Pre- and Post/R- methods was liable to having higher NPC contents than the corresponding pristine BC compared with the Post- method (**Fig. 5c**). The NPC contents of most Fe-BC were improved in the Pre- method possibly because (i) the presence of iron oxide as active agents contributed to the release of pyrolytic gases (*e.g.*, CO and CO_2) via the following reactions (Eq. 4-5), further promoting the formation of well-developed carbon structure [36, 54];

$$3Fe_2O_3 + C \rightarrow 2Fe_3O_4 + CO\uparrow \quad (4)$$

$$2Fe_2O_3 + 3C \rightarrow 4Fe^0 + 3CO_2\uparrow \quad (5)$$

(ii) the generated iron carbide or metallic iron during the thermal-reduction process of iron-soaked biomass could catalyze the graphitization of the carbon matrix [50]. In addition, the

increase of NPC in Fe-BC synthesized by the Post/R method might be attributed to the use of reductants, while the lower NPC contents were found in all Fe-BC produced by the Post- method (**Fig. 5c**).

Although the carbon content of biochar decreased after iron impregnation, the carbon content was the second influential factor in the Model BP (**Fig. 4a**). According to the PDP analysis, the carbon contents of BC and Fe-BC ranging from ~65% to ~75% facilitated Cr(VI) removal (**Fig. 3c**). NPC was identified as the third influential factor in the Model SF (**Fig. 4b**), further confirming the importance of carbon. The PDP curves of NPC decreased first and then increased with the increasing NPC until the turning point at ~70% (**Fig. 6c**). The decreasing trend of removal capacity when NPC ranged from ~50% to ~70% could be attributed to the decrease of SOFGs and poorly-developed aromatic structure [51]. In contrast, the enhanced electron transfer capacity of condensed graphitic structures and the improved electron-donating capacity with carbon defects could result in the upturn of removal capacity at high NPC contents (*i.e.*, NPC > 70%) [52, 53]. The carbon structural defects were mainly formed by high-temperature pyrolysis with the formation of graphitized carbon matrices, and they could significantly reduce Cr(VI) to stable Cr(III) [7, 37]. Moreover, well-developed biochar matrices would be more efficient for immobilizing active metal centers and reducing iron leaching, which may be conducive to Cr(VI) removal [7]. Therefore, high carbon contents with rich NPC proportion can also be a choice for the Fe-BC design, which may be attempted with the Pre- or Post/R- methods considering the performance and pros/cons of the three synthesis processes.

3.3.3 Roles of specific surface area in Cr(VI) removal

The biochar with a well-developed pore structure is indispensable for removing aqueous

pollutants. The variation of S_{BET} in Fe-BC showed a close correlation to the synthesis methods of Fe-BC. The cases of increase in S_{BET} after iron-impregnation accounted for 77%, 46%, 23% by the Pre-, Post- and Post/R- methods, respectively (**Fig. 5d**). There were multiple factors influencing S_{BET} variation in Fe-BC. For the Pre- method, the change of S_{BET} in Fe-BC could be attributed to (i) the formation and release of gaseous molecules (such as H_2O, CO, and CO_2) during the pyrolysis with iron contributed to a highly porous structure with more micropores, leading to the elevated S_{BET} in the Fe-BC [54]; (ii) the iron nanoparticles dispersed in the biochar structure may increase S_{BET} due to the large specific surface area of nanoparticles themselves [55]; and (iii) the possible iron aggregation and surface coverage would decrease S_{BET}, especially at high iron contents [56]. The loaded iron oxides on biochar either formed new surfaces or blocked original pores when using the Post- method, which may result in the nearly fifty-fifty ratio of S_{BET} increase or decrease in Fe-BC compared with pristine BC [57, 58]. The additional reduction step in the Post/R- method would reduce more iron to nano-sized Fe^0 grains with the following reaction (Eq. 6), which decreased S_{BET} of Fe-BC possibly because the generated Fe^0 nanoparticles were prone to blocking the micropores of biochar [59].

$$4Fe^{3+} + 3BH_4^- + 9H_2O \rightarrow 4Fe^0 + 3H_2BO_3^- + 6H_2\uparrow + 12H^+ \quad (6)$$

However, the specific BET surface area of BC and Fe-BC was the least influential factor for Cr(VI) removal among the studied material properties (**Fig. 4**). The minor influence of S_{BET} was reported and attributed to the reduction-dominated and adsorption-aided Cr(VI) removal mechanism [9]. The dependence of the removal capacity on S_{BET} still showed a significant increase, especially when S_{BET} was less than ~100 m^2/g (**Fig. 3d**), because the larger S_{BET} provided more interaction surface for biochar and Cr(VI). The trend of sustained increase

became trivial with a further rise of S_{BET} because the contents of active sites such as SOFGs and iron species on the biochar surface became the critical factors for improving Cr(VI) removal capacity [19, 60].

In general, the indirect impacts of impregnated iron on Cr(VI) removal by altering biochar properties were confirmed using the ML models in this study. The relative importance of these biochar properties for Cr(VI) removal can be ranked as follows: SOFGs > carbon structure > S_{BET}. For each indicator, the optimal proportion to remove Cr(VI) was identified, *i.e.*, O/C (from ~0.24 to ~0.32), C-O (from ~29% to ~38%), C=O (from 0 to ~25%), and NPC (less than 58% or more than 70%). The commonly used three methods for Fe-BC synthesis could promote the increase of O/C, but their influences on the other factors (*e.g.*, C-O/C=O, NPC, S_{BET}) were found to be variable. Therefore, the selection of synthesis methods should be carefully performed considering their influences on the Fe-BC properties, the roles of varying biochar properties in Cr(VI) removal, and the environmental impacts of the biochar synthesis.

4. Conclusions

This study investigated the variations of biochar properties after iron impregnation and analyzed the Cr(VI) removal capacity by BC and Fe-BC using a ML approach. Our results suggested that the direct impact of iron content on Cr(VI) removal capacity by Fe-BC was relatively low, possibly due to undistinguished Fe species in the models, but its indirect impacts were crucial. A higher O/C ratio was found in most Fe-BC after iron impregnation, which was identified as the most critical factor influencing Cr(VI) removal capacity. Based on the detailed information of SOFGs, the relative importance of C−O was higher by 19% than that of C=O

with different impact patterns on the removal of Cr(VI), and iron impregnation through post-reduction could create a higher ratio of C−O to C=O in the Fe-BC. Furthermore, the carbon contents of BC and Fe-BC ranging from ~65% to ~75% could better facilitate Cr(VI) removal. As the least factor influencing Cr(VI) removal, the specific BET surface area showed that the improvement of Cr(VI) removal would be limited when S_{BET} of BC and Fe-BC was higher than 100 m^2/g. The intrinsic information behind these ML models provided a useful reference for the design of engineered biochar under different application scenarios. The ML models can be further improved by distinguishing iron species, non-polar carbon species, and proportion of Cr(VI) reduction and adsorption in future research studies.

Acknowledgement

The authors appreciate the financial support from the Hong Kong Research Grants Council (PolyU 15222020), Hong Kong Environment and Conservation Fund (Project 101/2020), and Czech Science Foundation (Project 21-23794J) for this study.

Appendix A. Supplementary data

Supplementary data to this article can be found online at

References

[1] D. Hou, D. O'Connor, A.D. Igalavithana, D.S. Alessi, J. Luo, D.C. Tsang, D.L. Sparks, Y. Yamauchi, J. Rinklebe, Y.S. Ok, Metal contamination and bioremediation of agricultural soils for food safety and sustainability, Nat. Rev. Earth Environ. 1 (2020) 366-381.

[2] A.U. Rajapaksha, M. Vithanage, Y.S. Ok, C. Oze, Cr (VI) formation related to Cr (III)-muscovite and birnessite interactions in ultramafic environments, Environ. Sci. Technol. 47 (2013) 9722-9729.

[3] Z. Xu, X. Xu, Y. Zhang, Y. Yu, X. Cao, Pyrolysis-temperature depended electron donating and mediating mechanisms of biochar for Cr(VI) reduction, J. Hazard. Mater. 388 (2020) 121794.

[4] A.U. Rajapaksha, M.S. Alam, N. Chen, D.S. Alessi, A.D. Igalavithana, D.C. Tsang, Y.S. Ok, Removal of hexavalent chromium in aqueous solutions using biochar: chemical and spectroscopic investigations, Sci. Total Environ. 625 (2018) 1567-1573.

[5] S. Wang, M. Zhao, M. Zhou, Y.C. Li, J. Wang, B. Gao, S. Sato, K. Feng, W. Yin, A.D. Igalavithana, P. Oleszczuk, X. Wang, Y.S. Ok, Biochar-supported nZVI (nZVI/BC) for contaminant removal from soil and water: A critical review, J. Hazard. Mater. 373 (2019) 820-834.

[6] Y. Hu, X. Peng, Z. Ai, F. Jia, L. Zhang, Liquid Nitrogen Activation of Zero-Valent Iron and Its Enhanced Cr(VI) Removal Performance, Environ. Sci. Technol. 53 (2019) 8333-8341.

[7] Z. Wan, Y. Sun, D.C.W. Tsang, D. Hou, X. Cao, S. Zhang, B. Gao, Y.S. Ok, Sustainable remediation with an electroactive biochar system: mechanisms and perspectives, Green Chem. 22 (2020) 2688-2711.

[8] Y. Yi, Z. Huang, B. Lu, J. Xian, E.P. Tsang, W. Cheng, J. Fang, Z. Fang, Magnetic biochar for environmental remediation: A review, Bioresour. Technol. 298 (2020) 122468.

[9] Y. Yi, G. Tu, D. Zhao, P.E. Tsang, Z. Fang, Biomass waste components significantly influence the removal of Cr(VI) using magnetic biochar derived from four types of feedstocks and steel pickling waste liquor, Chem. Eng. J. 360 (2019) 212-220.

[10] Z. Wan, Y. Sun, D.C.W. Tsang, Z. Xu, E. Khan, S.-H. Liu, X. Cao, Sustainable impact of tartaric acid as electron shuttle on hierarchical iron-incorporated biochar, Chem. Eng. J. 395 (2020) 125138.

[11] Y. Sun, I.K.M. Yu, D.C.W. Tsang, X. Cao, D. Lin, L. Wang, N.J.D. Graham, D.S. Alessi, M. Komarek, Y.S. Ok, Y. Feng, X.D. Li, Multifunctional iron-biochar composites for the removal of potentially toxic elements, inherent cations, and hetero-chloride from hydraulic fracturing wastewater, Environ. Int. 124 (2019) 521-532.

[12] Z. Xu, X. Xu, D.C.W. Tsang, F. Yang, L. Zhao, H. Qiu, X. Cao, Participation of soil active components in the reduction of Cr(VI) by biochar: Differing effects of iron mineral alone and its combination with organic acid, J. Hazard. Mater. 384 (2020) 121455.

[13] J. Xu, Y. Yin, Z. Tan, B. Wang, X. Guo, X. Li, J. Liu, Enhanced removal of Cr(VI) by biochar with Fe as electron shuttles, J. Environ. Sci. (China) 78 (2019) 109-117.

[14] M.I. Jordan, T.M. Mitchell, Machine learning: Trends, perspectives, and prospects, Science 349 (2015) 255-260.

[15] X. Zhu, G. Wu, F.d.r. Coulon, L. Wu, D. Chen, Correlating asphaltene dimerization with its molecular structure by potential of mean force calculation and data mining, Energ. Fuel. 32 (2018) 5779-5788.

[16] X. Zhu, C.-H. Ho, X. Wang, Application of Life Cycle Assessment and Machine Learning for High-Throughput Screening of Green Chemical Substitutes, ACS Sustain. Chem. Eng. 8 (2020) 11141−11151.

[17] L. Breiman, Random forests, Mach. Learn. 45 (2001) 5-32.

[18] X. Zhu, X. Wang, Y.S. Ok, The application of machine learning methods for prediction of metal sorption onto biochars, J. Hazard. Mater. 378 (2019) 120727.

[19] X. Zhu, Z. Wan, D.C.W. Tsang, M. He, D. Hou, Z. Su, J. Shang, Machine learning for the selection of carbon-

based materials for tetracycline and sulfamethoxazole adsorption, Chem. Eng. J. 406 (2021) 126782.
[20] G. Sigmund, M. Gharasoo, T. Huffer, T. Hofmann, Deep Learning Neural Network Approach for Predicting the Sorption of Ionizable and Polar Organic Pollutants to a Wide Range of Carbonaceous Materials, Environ. Sci. Technol. 54 (2020) 4583-4591.
[21] X. Zhu, D.C.W. Tsang, L. Wang, Z. Su, D. Hou, L. Li, J. Shang, Machine learning exploration of the critical factors for CO_2 adsorption capacity on porous carbon materials at different pressures, J. Clean. Prod. 273 (2020) 122915.
[22] K. Zhang, S. Zhong, H. Zhang, Predicting Aqueous Adsorption of Organic Compounds onto Biochars, Carbon Nanotubes, Granular Activated Carbons, and Resins with Machine Learning, Environ. Sci. Technol. 54 (2020) 7008-7018.
[23] Z. Chen, D. Wei, Q. Li, X. Wang, S. Yu, L. Liu, B. Liu, S. Xie, J. Wang, D. Chen, T. Hayat, X. Wang, Macroscopic and microscopic investigation of Cr(VI) immobilization by nanoscaled zero-valent iron supported zeolite MCM-41 via batch, visual, XPS and EXAFS techniques, J. Clean. Prod. 181 (2018) 745-752.
[24] K. Sun, M. Kang, Z. Zhang, J. Jin, Z. Wang, Z. Pan, D. Xu, F. Wu, B. Xing, Impact of deashing treatment on biochar structural properties and potential sorption mechanisms of phenanthrene, Environ. Sci. Technol. 47 (2013) 11473-11481.
[25] N. Liu, Y. Zhang, C. Xu, P. Liu, J. Lv, Y. Liu, Q. Wang, Removal mechanisms of aqueous Cr(VI) using apple wood biochar: a spectroscopic study, J. Hazard. Mater. 384 (2020) 121371.
[26] M. Imran, Z.U.H. Khan, M.M. Iqbal, J. Iqbal, N.S. Shah, S. Munawar, S. Ali, B. Murtaza, M.A. Naeem, M. Rizwan, Effect of biochar modified with magnetite nanoparticles and HNO_3 for efficient removal of Cr (VI) from contaminated water: A batch and column scale study, Environ. Pollut. 261 (2020) 114231.
[27] S. Zhu, X. Huang, D. Wang, L. Wang, F. Ma, Enhanced hexavalent chromium removal performance and stabilization by magnetic iron nanoparticles assisted biochar in aqueous solution: Mechanisms and application potential, Chemosphere 207 (2018) 50-59.
[28] S. Ramanayaka, M. Vithanage, D.S. Alessi, W.-J. Liu, A.C.A. Jayasundera, Y.S. Ok, Nanobiochar: production, properties, and multifunctional applications, Environ. Sci. Nano 7 (2020) 3279-3302.
[29] X. Zhu, Y. Li, X. Wang, Machine learning prediction of biochar yield and carbon contents in biochar based on biomass characteristics and pyrolysis conditions, Bioresour. Technol. 288 (2019) 121527.
[30] S.B. Torrisi, M.R. Carbone, B.A. Rohr, J.H. Montoya, Y. Ha, J. Yano, S.K. Suram, L. Hung, Random forest machine learning models for interpretable X-ray absorption near-edge structure spectrum-property relationships, npj Comput. Mater. 6 (2020) 109.
[31] F. Pedregosa, G. Varoquaux, A. Gramfort, V. Michel, B. Thirion, O. Grisel, M. Blondel, P. Prettenhofer, R. Weiss, V. Dubourg, Scikit-learn: Machine learning in Python, J. Mach. Learn. Res. 12 (2011) 2825-2830.
[32] D. De Clercq, Z. Wen, F. Fei, L. Caicedo, K. Yuan, R. Shang, Interpretable machine learning for predicting biomethane production in industrial-scale anaerobic co-digestion, Sci. Total Environ. 712 (2020) 134574.
[33] M. Gusenbauer, H. Oezelt, J. Fischbacher, A. Kovacs, P. Zhao, T.G. Woodcock, T. Schrefl, Extracting local nucleation fields in permanent magnets using machine learning, npj Comput. Mater. 6 (2020) 89.
[34] D.G. Atinafu, B. Yeol Yun, Y. Uk Kim, S. Wi, S. Kim, Introduction of eicosane into biochar derived from softwood and wheat straw: Influence of porous structure and surface chemistry, Chem. Eng. J. 415 (2021) 128887.
[35] Y. Hu, G. Zhan, X. Peng, X. Liu, Z. Ai, F. Jia, S. Cao, F. Quan, W. Shen, L. Zhang, Enhanced Cr(VI) removal of zero-valent iron with high proton conductive $FeC_2O_4 \cdot 2H_2O$ shell, Chem. Eng. J. 389 (2020) 124414.
[36] L. Wu, S. Zhang, J. Wang, X. Ding, Phosphorus retention using iron (II/III) modified biochar in saline-

alkaline soils: Adsorption, column and field tests, Environ. Pollut. 261 (2020) 114223.
[37] J. He, Y. Xiao, J. Tang, H. Chen, H. Sun, Persulfate activation with sawdust biochar in aqueous solution by enhanced electron donor-transfer effect, Sci. Total Environ. 690 (2019) 768-777.
[38] Z. Xu, X. Xu, X. Tao, C. Yao, D.C.W. Tsang, X. Cao, Interaction with low molecular weight organic acids affects the electron shuttling of biochar for Cr(VI) reduction, J. Hazard. Mater. 378 (2019) 120705.
[39] H. Lyu, J. Tang, Y. Huang, L. Gai, E.Y. Zeng, K. Liber, Y. Gong, Removal of hexavalent chromium from aqueous solutions by a novel biochar supported nanoscale iron sulfide composite, Chem. Eng. J. 322 (2017) 516-524.
[40] M.L. Erickson, S.M. Elliott, C.J. Brown, P.E. Stackelberg, K.M. Ransom, J.E. Reddy, C.A. Cravotta, Machine-Learning Predictions of High Arsenic and High Manganese at Drinking Water Depths of the Glacial Aquifer System, Northern Continental United States, Environ. Sci. Technol. 55 (2021) 5791–5805 .
[41] L. Wu, S. Zhang, J. Wang, X. Ding, Phosphorus retention using iron (II/III) modified biochar in saline-alkaline soils: Adsorption, column and field tests, Environ. Pollut. 261 (2020) 114223.
[42] Y. Zhang, X. Jiao, N. Liu, J. Lv, Y. Yang, Enhanced removal of aqueous Cr(VI) by a green synthesized nanoscale zero-valent iron supported on oak wood biochar, Chemosphere 245 (2020) 125542.
[43] X. Xu, H. Huang, Y. Zhang, Z. Xu, X. Cao, Biochar as both electron donor and electron shuttle for the reduction transformation of Cr(VI) during its sorption, Environ. Pollut. 244 (2019) 423-430.
[44] M. Chen, F. He, D. Hu, C. Bao, Q. Huang, Broadened operating pH range for adsorption/reduction of aqueous Cr(VI) using biochar from directly treated jute (Corchorus capsularis L.) fibers by H_3PO_4, Chemical Engineering Journal 381 (2020) 122739.
[45] P.C. Bandara, J. Pena-Bahamonde, D.F. Rodrigues, Redox mechanisms of conversion of Cr(VI) to Cr(III) by graphene oxide-polymer composite, Sci. Rep. 10 (2020) 9237.
[46] Y. Huang, X. Lee, F.C. Macazo, M. Grattieri, R. Cai, S.D. Minteer, Fast and efficient removal of chromium (VI) anionic species by a reusable chitosan-modified multi-walled carbon nanotube composite, Chemi. Eng. J. 339 (2018) 259-267.
[47] W.-D. Oh, T.-T. Lim, Design and application of heterogeneous catalysts as peroxydisulfate activator for organics removal: An overview, Chem. Eng. J. 358 (2019) 110-133.
[48] F. Martins, S. Machado, T. Albergaria, C. Delerue-Matos, LCA applied to nano scale zero valent iron synthesis, Int. J. Life Cycle Assess. 22 (2017) 707-714.
[49] T. Sun, B.D.A. Levin, M.P. Schmidt, J.J.L. Guzman, A. Enders, C.E. Martinez, D.A. Muller, L.T. Angenent, J. Lehmann, Simultaneous Quantification of Electron Transfer by Carbon Matrices and Functional Groups in Pyrogenic Carbon, Environ. Sci. Technol. 52 (2018) 8538-8547.
[50] K. Lotz, A. Wutscher, H. Dudder, C.M. Berger, C. Russo, K. Mukherjee, G. Schwaab, M. Havenith, M. Muhler, Tuning the Properties of Iron-Doped Porous Graphitic Carbon Synthesized by Hydrothermal Carbonization of Cellulose and Subsequent Pyrolysis, ACS Omega 4 (2019) 4448-4460.
[51] Z. Xu, X. Xu, Y. Yu, C. Yao, D.C.W. Tsang, X. Cao, Evolution of redox activity of biochar during interaction with soil minerals: Effect on the electron donating and mediating capacities for Cr(VI) reduction, J. Hazard. Mater. 414 (2021) 125483.
[52] Y. Yuan, N. Bolan, A. Prevoteau, M. Vithanage, J.K. Biswas, Y.S. Ok, H. Wang, Applications of biochar in redox-mediated reactions, Bioresour. Technol. 246 (2017) 271-281.
[53] L. Klupfel, M. Keiluweit, M. Kleber, M. Sander, Redox properties of plant biomass-derived black carbon (biochar), Environ. Sci. Technol. 48 (2014) 5601-5611.
[54] S. Zeng, Y.K. Choi, E. Kan, Iron-activated bermudagrass-derived biochar for adsorption of aqueous sulfamethoxazole: Effects of iron impregnation ratio on biochar properties, adsorption, and regeneration, Sci.

Total Environ. 750 (2021) 141691.

[55] D. Ma, Y. Yang, B. Liu, G. Xie, C. Chen, N. Ren, D. Xing, Zero-valent iron and biochar composite with high specific surface area via K2FeO4 fabrication enhances sulfadiazine removal by persulfate activation, Chem. Eng. J. 408 (2021) 127992.

[56] S. Yuan, M. Hong, H. Li, Z. Ye, H. Gong, J. Zhang, Q. Huang, Z. Tan, Contributions and mechanisms of components in modified biochar to adsorb cadmium in aqueous solution, Sci. Total Environ. 733 (2020) 139320.

[57] A.G. Karunanayake, O.A. Todd, M.L. Crowley, L.B. Ricchetti, C.U. Pittman, R. Anderson, T.E. Mlsna, Rapid removal of salicylic acid, 4-nitroaniline, benzoic acid and phthalic acid from wastewater using magnetized fast pyrolysis biochar from waste Douglas fir, Chem. Eng. J. 319 (2017) 75-88.

[58] Y. Zhu, H. Li, G. Zhang, F. Meng, L. Li, S. Wu, Removal of hexavalent chromium from aqueous solution by different surface-modified biochars: Acid washing, nanoscale zero-valent iron and ferric iron loading, Bioresour. Technol. 261 (2018) 142-150.

[59] M. Ahmed, J. Zhou, H. Ngo, W. Guo, M. Johir, K. Sornalingam, D. Belhaj, M. Kallel, Nano-Fe^0 immobilized onto functionalized biochar gaining excellent stability during sorption and reduction of chloramphenicol via transforming to reusable magnetic composite, Chem. Eng. J., 322 (2017) 571-581.

[60] K. Liu, F. Li, X. Zhao, G. Wang, L. Fang, The overlooked role of carbonaceous supports in enhancing arsenite oxidation and removal by nZVI: Surface area versus electrochemical property, Chem. Eng. J. 406 (2021) 126851.

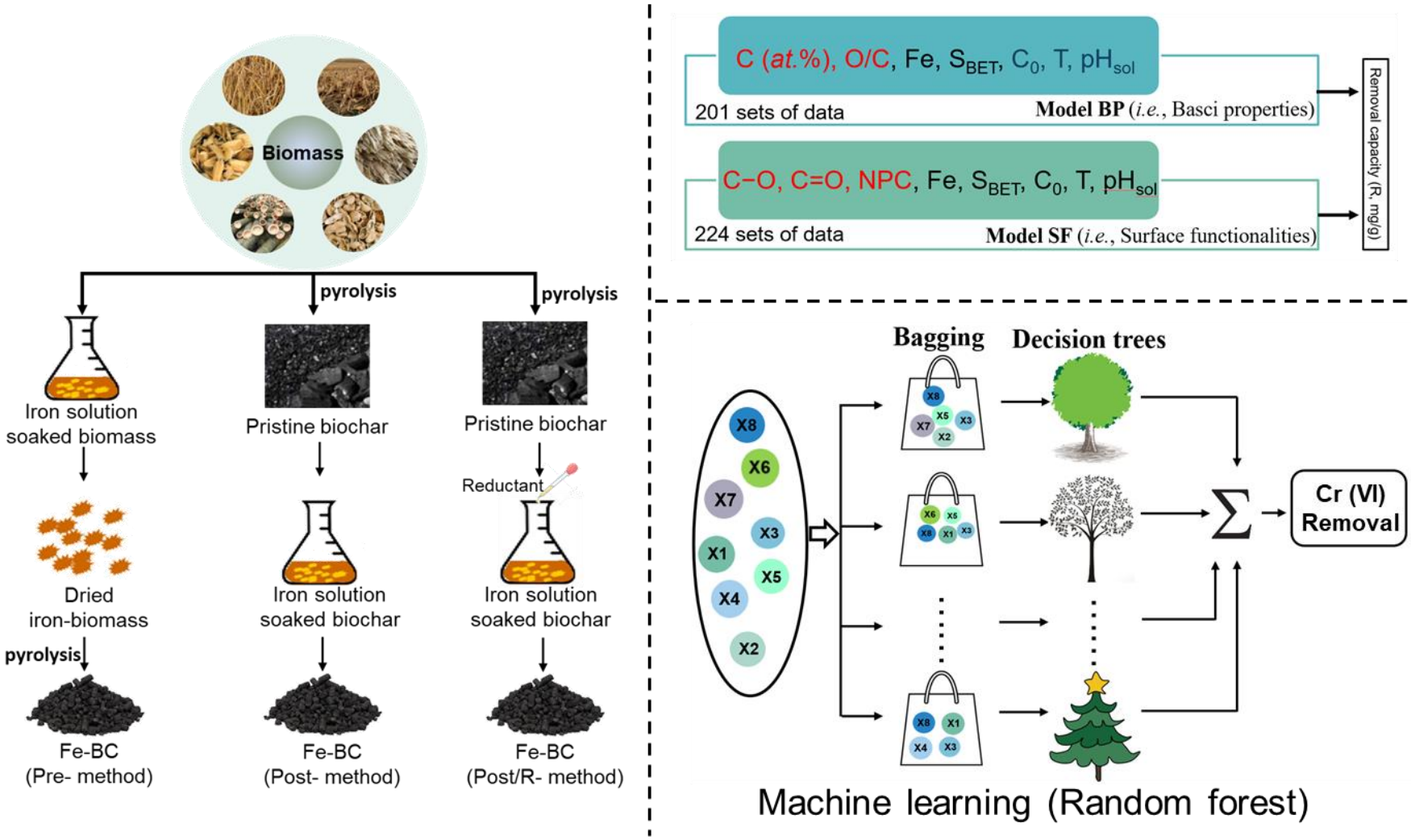

Fig. 1 Three most widely-used methods of iron-biochar synthesis and the framework of the research.

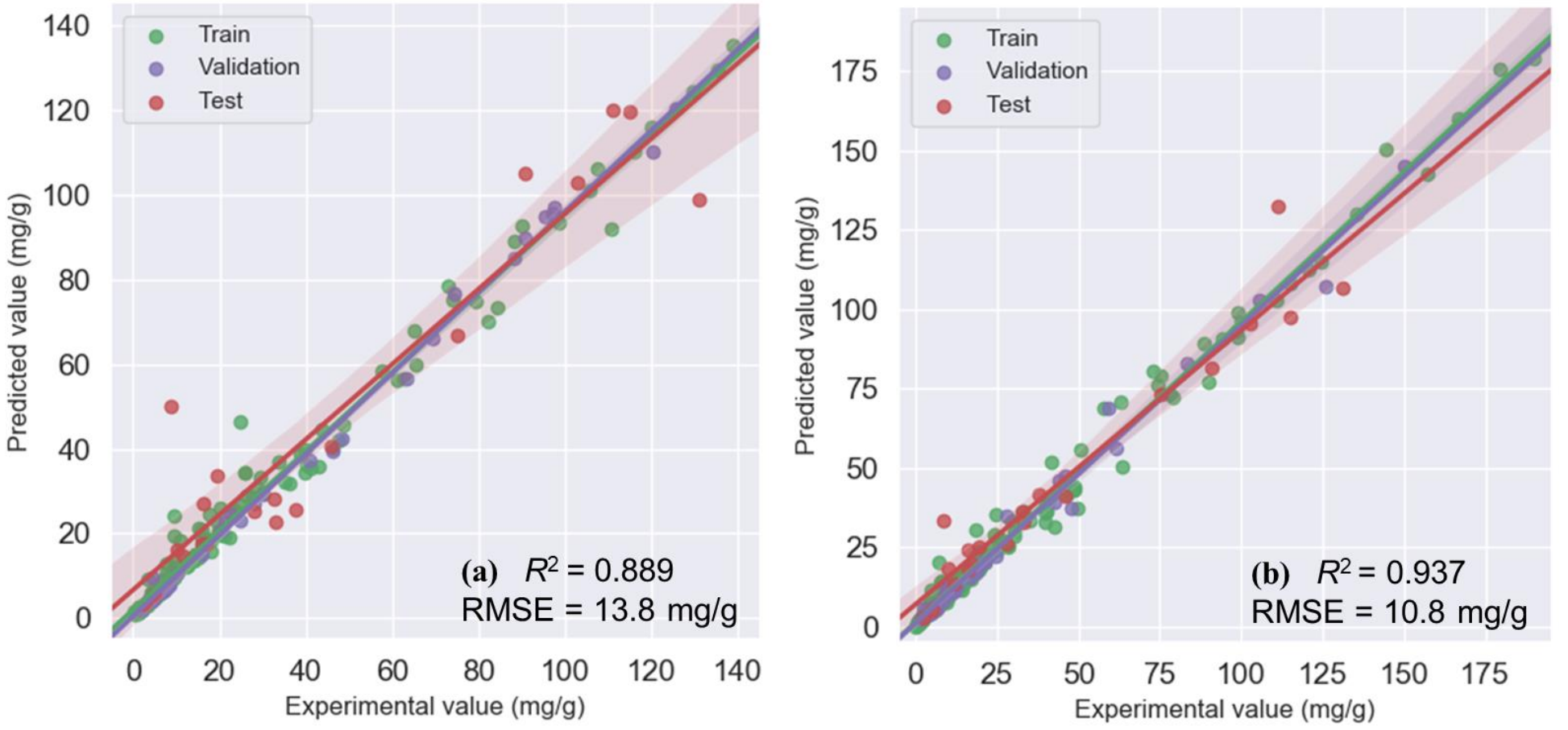

Fig. 2 Predicted removal capacity versus experimentally determined removal capacity values with (a) Model BP and (b) Model SF. The lines represent the regression line and the shaded area indicate 95% confidence interval. The R^2 and RMSE were calculated based on the prediction in the test group.

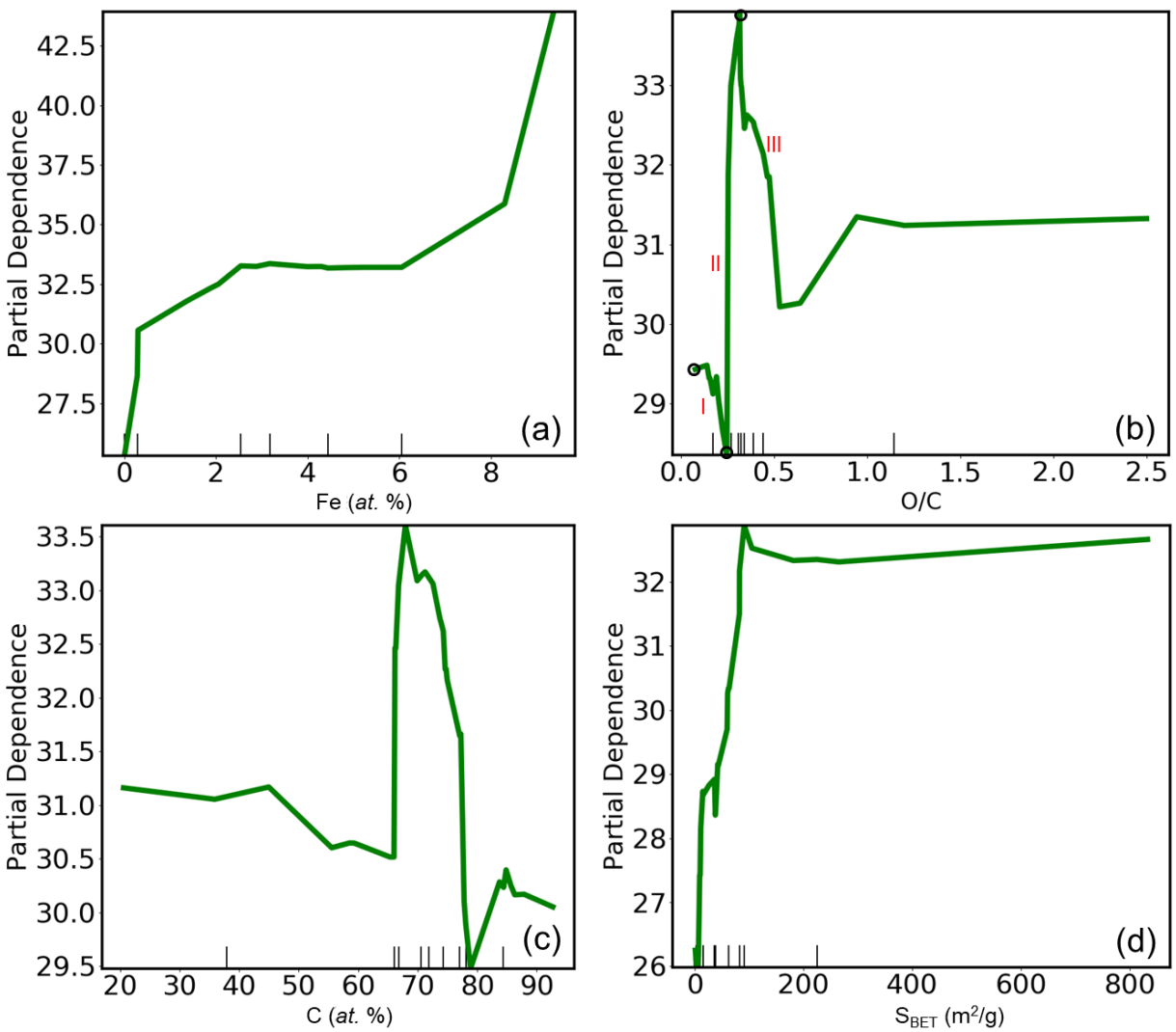

Fig. 3 Partial dependence plots of Cr(VI) removal capacity on material properties in Model BP. The pikes on the x-axis represent the fractile of feature values and reflected the data density.

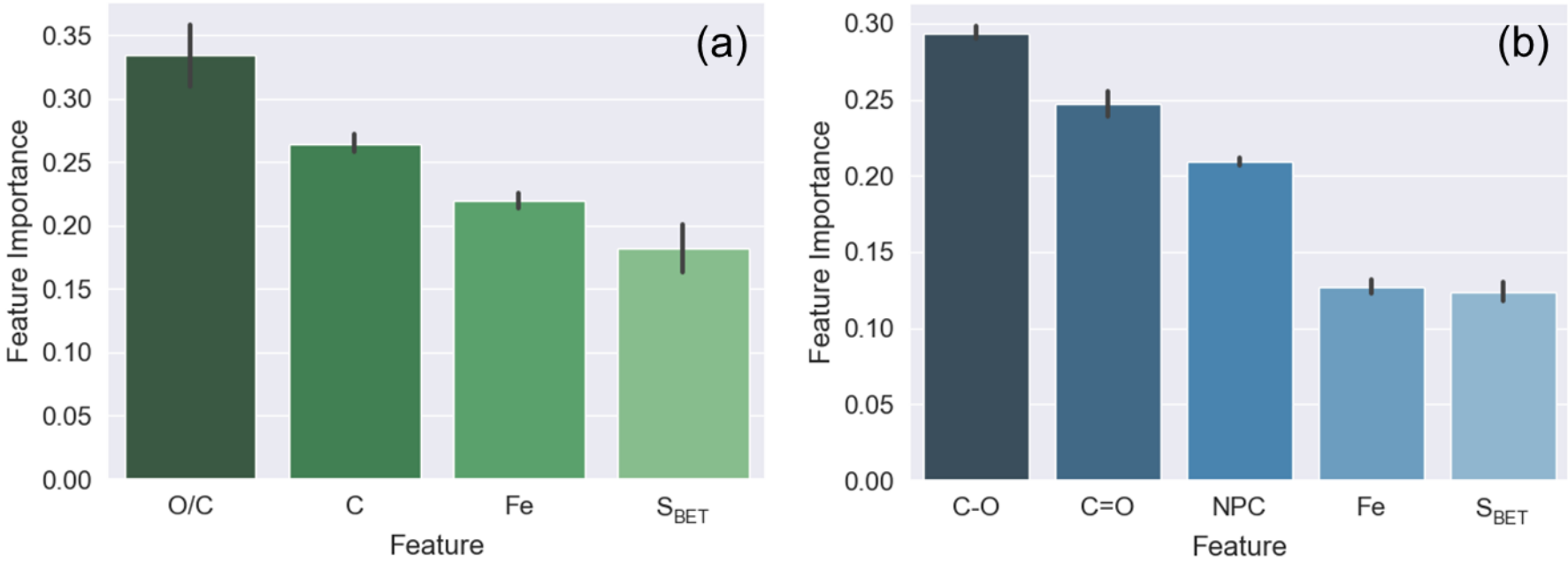

Fig. 4 Importance rank of material properties to Cr(VI) removal capacity by biochar and iron-biochar in (a) Model BP and (b) Model SF.

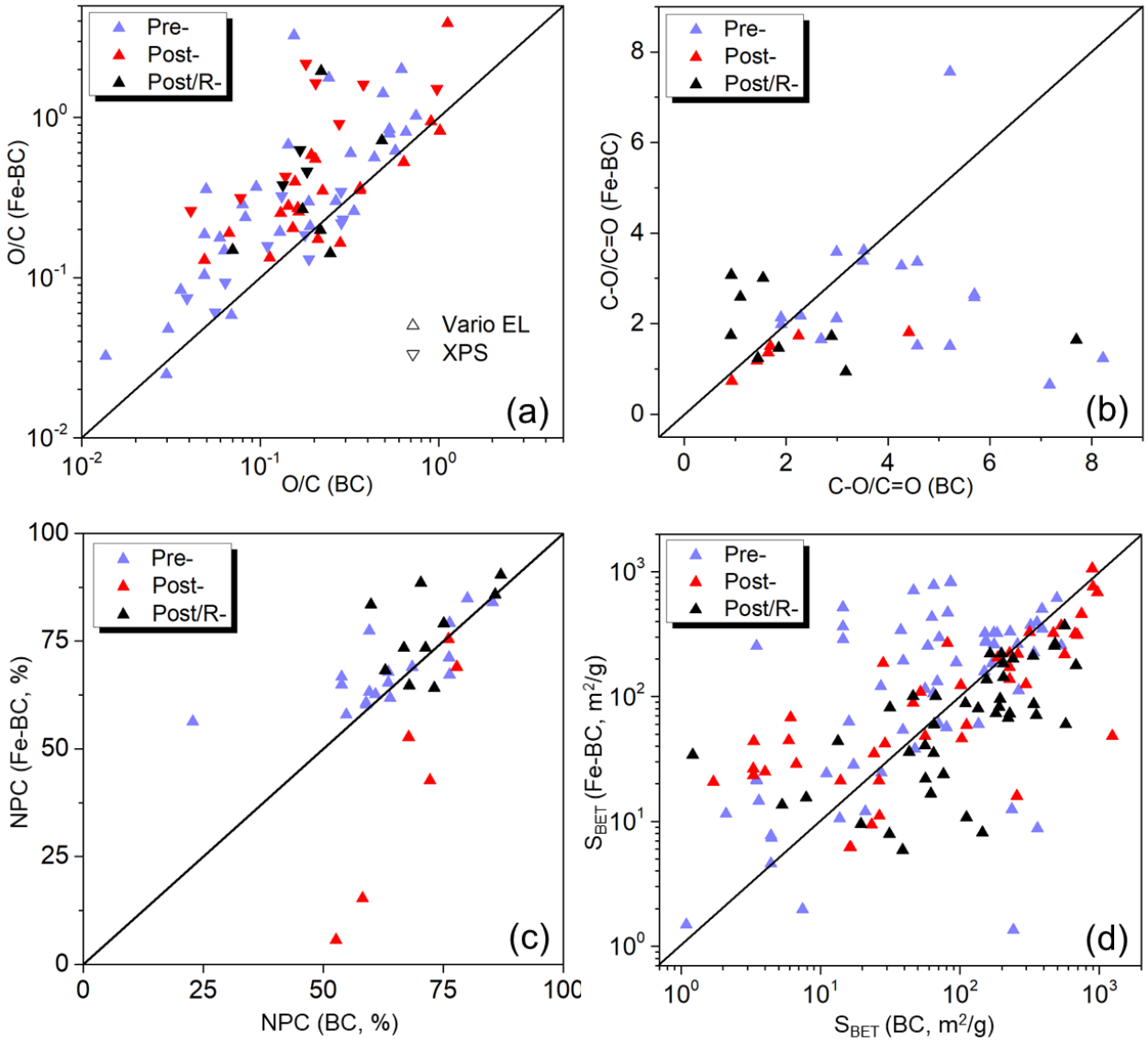

Fig. 5 Reported changes of biochar properties due to the different iron-loading methods: (a) the atomic ratio of oxygen to carbon (O/C); (b) the ratio of C−O to C=O (C−O/C=O); (c) the relative proportion of non-polar C (NPC); (d) specific surface area (S_{BET}). The Pre-, Post-, and Post/R- represent directly pyrolysis of iron-soaked biomass, co-precipitation of biochar and ferric/ferrous salts in alkali solution, and liquid-phase reduction of iron by borohydride on biochar surface. Vario EL and XPS indicate the O/C measured by elemental analyzer and XPS, respectively. The references are provided in SI Table S1.

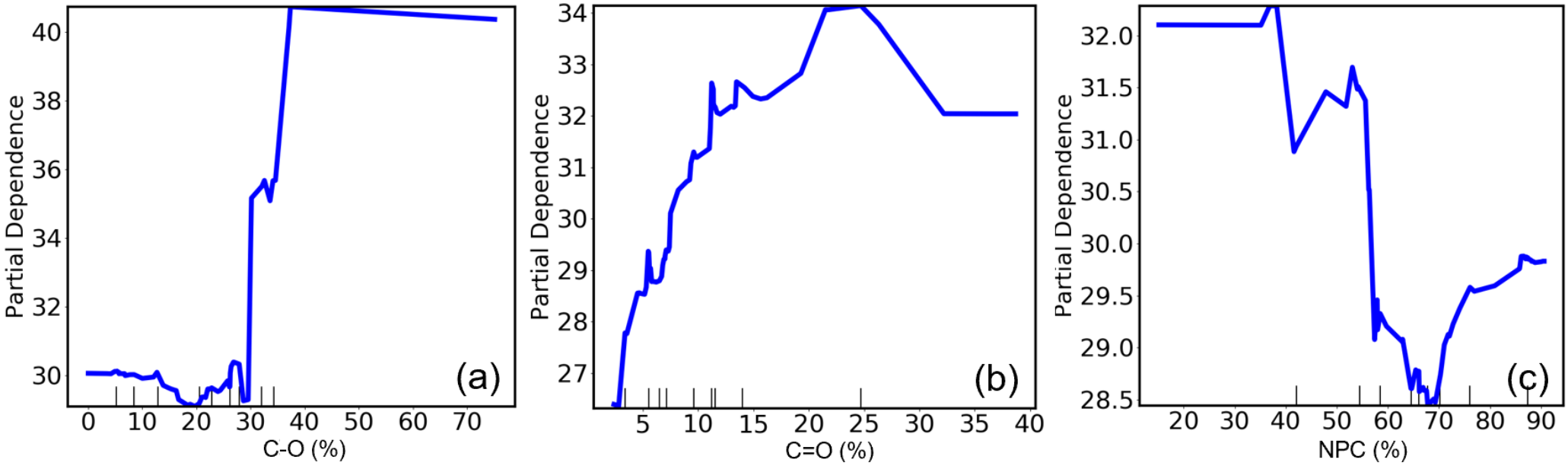

Fig. 6 Partial dependence plots of Cr(VI) removal capacity on surface functional groups of biochar in Model SF. The pikes on the x-axis represent the fractile of feature values and reflected the data density.